

Bipartite phosphoinositide-dependent modulation of auxin signaling during xylem differentiation in *Arabidopsis thaliana* roots

Journal Article**Author(s):**

von der Mark, Claudia; Cruz, Tiago M.D.; Blanco-Touriñán, Noel; Rodriguez-Villalon, Antia

Publication date:

2022-12

Permanent link:

<https://doi.org/10.3929/ethz-b-000572543>

Rights / license:

[Creative Commons Attribution-NonCommercial 4.0 International](#)

Originally published in:

New Phytologist 236(5), <https://doi.org/10.1111/nph.18448>

Funding acknowledgement:

160201 - Phosphoinositides- Molecular analysis of new lipid regulators in plant phloem differentiation (SNF)

Bipartite phosphoinositide-dependent modulation of auxin signaling during xylem differentiation in *Arabidopsis thaliana* roots

Claudia von der Mark , Tiago M. D. Cruz, Noel Blanco-Tourinán  and Antia Rodriguez-Villalon 

Department of Biology, Swiss Federal Institute of Technology (ETH) Zurich, CH-8092, Zurich, Switzerland

Authors for correspondence:

Antia Rodriguez-Villalon

Email: antia.rodriguez@biol.ethz.ch

Claudia von der Mark

Email: claudia.vondermark@biol.ethz.ch

Received: 21 January 2022

Accepted: 14 August 2022

New Phytologist (2022) 236: 1734–1747

doi: 10.1111/nph.18448

Key words: *Arabidopsis thaliana*, auxin transport, cell differentiation, nuclear phosphoinositides, root, secondary cell wall, vascular development, xylem formation.

Summary

- Efficient root-to-shoot delivery of water and nutrients in plants relies on the correct differentiation of xylem cells into hollow elements. While auxin is integral to the formation of xylem cells, it remains poorly characterized how each subcellular pool of this hormone regulates this process.
- Combining genetic and cell biological approaches, we investigated the bipartite activity of nucleoplasmic vs plasma membrane-associated phosphatidylinositol 4-phosphate kinases PIP5K1 and its homolog PIP5K2 in *Arabidopsis thaliana* roots and uncovered a novel mechanism by which phosphoinositides integrate distinct aspects of the auxin signaling cascade and, in turn, regulate the onset of xylem differentiation.
- The appearance of undifferentiated cells in protoxylem strands of *pip5k1 pip5k2* is phenomimicked in auxin transport and perception mutants and can be partially restored by the nuclear residence of PIP5K1. By contrast, exclusion of PIP5K1 from the nucleus hinders the auxin-mediated induction of the xylem master regulator *VASCULAR RELATED NAC DOMAIN (VND) 7*. A xylem-specific increase of auxin levels abolishes *pip5k1 pip5k2* vascular defects, indicating that the establishment of auxin maxima is required to activate *VND7*-mediated xylem differentiation.
- Our results describe a new mechanism by which distinct subcellular pools of phosphoinositides integrate auxin transport and perception to initiate xylem differentiation in a spatiotemporal manner.

Introduction

In *Arabidopsis thaliana* (*Arabidopsis*), as in all higher plants, xylem vessels are essential for the transport of water and nutrients absorbed by the root to the aboveground organs. The appearance of xylem vessels facilitating long-distance transport among separated organs was key in plant evolution from bryophytes to trees and has enabled the conquest of the land by plants (Lucas *et al.*, 2013). Within *Arabidopsis* roots, two protoxylem strands are positioned at the outermost position of the stele, between which three metaxylem files develop (Fig. 1a–c; Dolan *et al.*, 1993). To form a continuous system of adjoining hollowed elements, xylem cells undergo a complex and fine-tuned developmental program which starts with xylem specification, followed by cell proliferation, elongation and eventually terminal differentiation (De Rybel *et al.*, 2016; Ruonala *et al.*, 2017). Differentiation of xylem cells involves autolysis and the deposition of a secondary cell wall (SCW) comprising highly polymerized cellulose and lignin (Bollhoner *et al.*, 2012; Escamez & Tuominen, 2014). Secondary cell wall assembly occurs in an annular/spiral or pitted/reticulated pattern in the case of protoxylem or metaxylem cells respectively

(Fig. 1a,c; Oda & Fukuda, 2012). Autolysis in xylem cells initiates with the rupture of the vacuole, which releases proteolytic enzymes into the cytosol, reducing the cytosolic pH and creating an optimal environment for organelle degradation (Bollhoner *et al.*, 2012; Escamez & Tuominen, 2014). Members of the *VASCULAR RELATED NAC DOMAIN (VND)* transcription factor family *VND1–7* have been found to interact at the transcriptional and protein level (Yamaguchi *et al.*, 2008; Escamez & Tuominen, 2014), hence forming an interconnected network of xylem developmental master regulators with distinct effects on xylem formation (Yamaguchi *et al.*, 2008; Endo *et al.*, 2015). Ubiquitous overexpression of *VND6* or *VND7* is sufficient to induce ectopic formation of metaxylem or protoxylem cells respectively, while *VND1–3* were recently associated with abscisic acid (ABA)-mediated metaxylem development in *Arabidopsis* roots (Kubo *et al.*, 2005; Ramachandran *et al.*, 2021). In protoxylem cells, the deposition of lignin and hemicellulose in the SCW are regulated by *VND7* in a dose-dependent manner with features of hysteresis (Yamaguchi *et al.*, 2008; Turco *et al.*, 2019). *VND7* induction triggers the expression of a multitude of transcription factors and enzymes involved in xylem differentiation, including *MYB*

DOMAIN PROTEIN 46 (MYB46) (Zhong *et al.*, 2010), which in turn activates a transcriptional cascade that includes lignin and cellulose biosynthetic enzymes as well as hydrolytic enzymes (Kim *et al.*, 2013).

It is well accepted that auxin plays an integral role in the formation of xylem tissues, as described in transdifferentiation assays and studies performed in cultures of *Zinnia elegans* (Kubo *et al.*, 2005; Cano-Delgado *et al.*, 2010; De Rybel *et al.*, 2016). Perception of auxin by the nuclear TRANSPORT INHIBITOR RESPONSE 1 (TIR1) or AUXIN SIGNALING F-BOX (AFB) receptors triggers the proteasome-mediated degradation of auxin/indole-3-acetic acid (AUX/IAA) repressors, enabling the transcription of *AUXIN RESPONSIVE FACTOR (ARF)* genes involved in regulating auxin responses (Strader & Zhao, 2016). Within the root vascular cylinder, the directional cell-to-cell flow of auxin is maintained by the polar distribution of auxin efflux carriers such as PIN-FORMED (PIN)1, PIN3, PIN4 and PIN7 (Bishopp *et al.*, 2011). To promote auxin transport, PIN1 activity depends on the plasma membrane-lipidic composition. In particular, the accumulation of phosphatidylinositol 4,5-bis-phosphate (PtdIns(4,5)P₂) appears to be crucial for proper PIN1 localization in epidermal cells (Ischebeck *et al.*, 2013; Tejos *et al.*, 2014). Remarkably, a genetically induced enrichment of PtdIns(4,5)P₂ at the plasma membrane (PM) accelerates protoxylem differentiation by enhancing cell trafficking towards the vacuoles (Gujas *et al.*, 2017). Augmented levels of PtdIns(4,5)P₂ specifically at the PM of protoxylem cells trigger the premature expression of protoxylem genes associated with vascular differentiation such as the transcription factor *MYB46* (Gujas *et al.*, 2017). Notably, one biosynthetic phosphatidylinositol 4-phosphate 5-kinase (PIP5K) 2 has been recently described to accumulate in the nuclei of epidermal cells (Gerth *et al.*, 2017), implying the existence of distinct subcellular PtdIns(4,5)P₂ pools. Yet, uncovering the role of distinct PtdIns(4,5)P₂ subcellular pools in xylem development has been hampered thus far by the technical limitations imposed by the localization of xylem cells in the innermost part of the root.

In this study, we show that the activities of PIP5K2 and its homologous PIP5K1 are essential for xylem differentiation, as revealed by the interrupted vascular strands observed in *pip5k1 pip5k2* double mutants. Similar phenotypes were observed upon chemical or genetic restriction of auxin transport and perception, indicating that PIP5Ks participate in channeling auxin through and to xylem cells. Exclusion of PIP5K1 from the nucleus disturbs xylem formation, whereas its accumulation specifically in the nuclear compartment diminishes *pip5k1 pip5k2* vascular defects. The appearance of protoxylem gap cells (PGCs) in the aforementioned mutants correlates with the absence of *VND7* expression and its downstream targets in these cells, implying that an optimal auxin peak is required to activate *VND7*. Indeed, an increase in auxin levels by introgression of auxin biosynthetic enzymes restores xylem continuity in *pip5k1 pip5k2* roots. While our results imply that a boost of auxin levels is necessary to initiate a *VND7*-dependent xylem differentiation, the xylem-deficient phenotype observed in *vnd7 vnd6* double mutants reflects defects in the upstream activation of *VND7* spanning beyond auxin. Indeed, despite the lack of an auxin maximum, *VND3* expression

as well as transcripts from other protoxylem-associated genes can still be detected in *pip5k1 pip5k2* xylem gap cells, suggesting that protoxylem identity is established in those cells. Our results show a novel mechanism by which plants modulate the entry of xylem differentiation at subcellular resolution by synchronizing diverse aspects of the auxin signaling cascade at the single-cell level.

Materials and Methods

Plant material and growth conditions

All plants used in this study were from the *A. thaliana* ecotype *Col-0*. The mutant alleles used in the course of the present study were previously described elsewhere: *pip5k1 pip5k2* (Tejos *et al.*, 2014), *tir1-1 abf2-1 abf3-1* (Mazur *et al.*, 2020b), *pin3 pin4 pin7* (Friml *et al.*, 2003), and *vnd6 vnd7* and *vnd1 vnd3* (Haseloff, 1999). Translational fusion and reporter markers used in this study were kindly provided by Drs Dolf Weijers (*UBQ::R2D2*; Liao *et al.*, 2015), Thomas Greb (*VND7::GFP*), Taku Demura (*VND1::GUS*, *VND3::GUS*, *VND6::GUS* and *VND7::GUS*), Bert de Rybel (*TMO5::TMO5-n3GFP*), Takashi Aoyama (*PIP5K1::PIP5K1:YFP*) and Clara Sanchez-Rodriguez (*35S::VND7::V16-GR*, *PIP5K2::XVE:PIP5K2-YFP*). *xcp1* (*SALK_084789*), *xcp2* (*SALK_010938*), *myb46* (*SALK_88514*), *myb83* (*SALK_093099C*) and *cesa8* (*SALK_026812; irx1-5*) T-DNA insertion lines were obtained from NASC and crossed to generate the respective double mutants.

Seeds were stratified in the dark at 4°C for 48 h and grown on vertically orientated ½ Murashige & Skoog (½MS) medium plates under continuous light conditions in a walk-in growth chamber. The 48 and 24 h treatments were performed on 4- and 5-d-old seedlings, respectively, grown on ½MS plates and then transferred to plates supplemented with the indicated amounts of estradiol (ES), auxinole, 1-*N*-naphthylphthalamic acid (NPA) and dexamethasone (DEX). All chemical compounds were obtained from Sigma-Aldrich and dissolved in DMSO or water following the manufacturer's indications, with the exception of auxinole (provided by Dr Hiroshi Nozaki).

Cloning and plant transformation

Unless stated otherwise, all constructs were generated using the double or triple Multi-Site Gateway system following the handbook instructions. To clone *AHP6* and *CESA7* promoters, 2 kb genomic DNA regions were PCR-amplified using the primers listed in Supporting Information Table S1 and introduced in pMDC7 (Invitrogen) by digestion-ligation using *PmaI/BstBI* restriction sites. Coding sequences of *PIP5K1-FL*, *PIP5K1^{AMORN}* and *3XNLS-PIP5K1* were *in vitro* synthesized and then introduced in pMDC37 vector to generate green fluorescent protein (GFP) translational fusion versions. To generate the PIP5K1 translational reporter line, 2 kb of the genomic DNA region was amplified using the primers listed in Table S1. Together with the previously amplified coding sequence of PIP5K1, both PCR-amplified products were introduced and finally recombined together with pENTRY-CITRINE into pH7m34GW plasmid following the

Gateway handbook instructions (Gujas *et al.*, 2017). *AHP6::XVE:shy2-2* and *CESA7::XVE:shy2-2* lines were generated by the recombination of *pENTRY-shy2-2* (Vermeer *et al.*, 2014) with the respective *AHP6::XVE* or *CESA7::XVE*-containing destination vector (Gujas *et al.*, 2017). To amplify *YUCCA2*, *YUCCA8* and *TSB1*, the coding sequence of these proteins was amplified using the primers listed in Table S1 and the resulting PCR products were introduced into pDNR221 Gateway vectors. The resulting *pENTRY-YUCCA* and *pENTRY-TSB1* were recombined with the above-described *AHP6::XVE* and *UBQ::XVE* vectors following handbook instructions. Transgenic plants were generated using floral-dip transformation techniques as previously described (Gujas *et al.*, 2017). At least six independent insertion events were analyzed for each transgenic line to ensure reproducibility. Introgression of reporter lines into the *pip5k1 pip5k2* genetic background was performed by crossing.

Reverse transcription quantitative PCR

RNA extraction, cDNA synthesis and reverse transcription quantitative PCR (RT-qPCR) were performed as previously described (Kastanaki *et al.*, 2022). Two biological replicates were analyzed, each including three technical replicates. The following primers were used: PDF2_Fw, 5'-TAACGTGGCCAAAATGATGC-3'; PDF2_Rv, 5'-GTTCTCCACAACCGCTTGGT-3' (Czechowski *et al.*, 2005), RT-AHP6_Fw, 5'-GTGCTTGAGAGACTGGAGG-3', RT-AHP6_Rv, 5'-TACATTGGATATCTGACTCCTG-3' (Jang *et al.*, 2017). *PDF2* was used as a reference gene and relative expression values were calculated using the $\Delta\Delta C_T$ method.

Histology, GUS staining and transient expression in *Nicotiana benthamiana*

To obtain cross-sections of 6-d-old *Arabidopsis* vascular tissues, Col-0 and *pip5k1 pip5k2* roots were embedded in plastic resin and sliced as described previously (Rodriguez-Villalon *et al.*, 2015) with slight modification. Before embedding, roots were fixed overnight at 4°C in a solution containing 1% glutaraldehyde, 4% formaldehyde, 0.1% Triton and 0.05 M sodium phosphate buffer (NaPi) pH 7.2. After mounting on the slide, cross-sections were stained using 0.05% Toluidine blue solution. Histochemical β -glucuronidase (GUS) staining was performed according to Jefferson *et al.* (1987). For visualization of nuclear and PM versions of PIP5K1, we transformed *Agrobacterium tumefaciens* and transformed leaves following Norkunas *et al.* (2018).

Microscopy and phenotype analysis

Analysis of root xylem phenotypes was performed using 6-d-old seedlings, cleared and fixed using a ClearSee protocol described elsewhere (Kurihara *et al.*, 2015). Before microscopy, seedlings were stained with Basic Fuchsin (0.2%) dye for *c.* 16 h and Calcofluor White (0.01%) for 1 h. Roots were then mounted in ClearSee solution and immediately visualized. Visualization of fuchsin-stained roots was carried out using 561 nm excitation

and 560–650 nm emission. Phenotypical quantification was carried out by assessing the xylem defects in each root and representing the frequency of a certain defect in a plant population. To image protein localization with virtual cross-sections of the stele, 6-d-old seedlings containing fusion proteins were stained with 10 $\mu\text{g ml}^{-1}$ propidium iodide (PI; Sigma-Aldrich) and imaged by confocal (Zeiss LSM 780 instrument) or multiphoton (Leica SP8 instrument; Leica TCS SP8 MP, Wetzlar, Germany) microscopes (488 nm excitation and 505–565 nm emission). Representative images of each experiment are displayed, and images of the same panel were represented with comparable objective magnification and zoom. 4',6-Diamidino-2-phenylindole dihydrochloride (DAPI) nuclear staining was performed using DAPI (20 $\mu\text{g ml}^{-1}$) dissolved in a solution of H₂O and 0.5% (v/v) Triton X-100. Seedlings were incubated for 30 min in DAPI solution during Fuchsin Basic washing steps (405 nm excitation and 425–475 nm emission). To analyze the ratio of mDII-ntd-Tomato : DII-GFP, R2D2 green and red fluorophores were excited at 488 and 561 nm and detected between 495–550 and 575–635 nm, respectively. To measure the ratio of fluorophores, analysis was performed as in Liao *et al.* (2015). Briefly, 6-d-old seedlings germinated in $\frac{1}{2}$ MS plates were soaked in 4 ml of liquid $\frac{1}{2}$ MS media with the indicated amounts of naphthaleneacetic acid (NAA) or NPA for 4 h. Ratio values were obtained by measuring the area of nuclei using IMAGEJ software, followed by subtraction of background intensity using the same area. Means and standard error were calculated and statistical significance was evaluated by Tukey's pairwise comparison test. To perform transdifferentiation of root cells into xylem differentiated elements in *35S::VND7-VPI6-GR*, 6-d-old plants were incubated with DEX for 48 h and fixed for 1 h in 4% paraformaldehyde (PFA) and stained for *c.* 1 h with Calcofluor White (0.01%) before imaging.

Results

PIP5K1 and PIP5K2 activities are required for the differentiation of xylem tissues

To gain better insight into the role of PtdIns(4,5)P₂ in modulating xylem formation, we analyzed whether this process is altered in *pip5k1 pip5k2* mutants. Xylem formation can be visualized by the deposition of cellulose and lignin in the SCW of vascular cells, which can be scored by using specific polymer-binding dyes such as Calcofluor White, fuchsin or toluidine blue (Fig. 1a). Histological examination of cross-sections of toluidine blue-stained roots showed the appearance of SCW-devoid cells at protoxylem positions in *pip5k1 pip5k2*, hereafter referred to as PGCs (Fig. 1a–f). Similar results were obtained when analyzing *pip5k1 pip5k2* roots stained with fuchsin by confocal microscopy (Fig. 1g–h',y), whereas this phenotype was rarely observed in the wild-type (WT; Fig. 1b,c,g,g',y). In 3- and 4-d-old seedlings, xylem breaks often appeared close to the meristematic region, which we named region 1 (Figs 1a, S1C). By contrast, 6-d-old seedlings often exhibit discontinuous protoxylem strands in regions 2 and 3, where metaxylem cell files

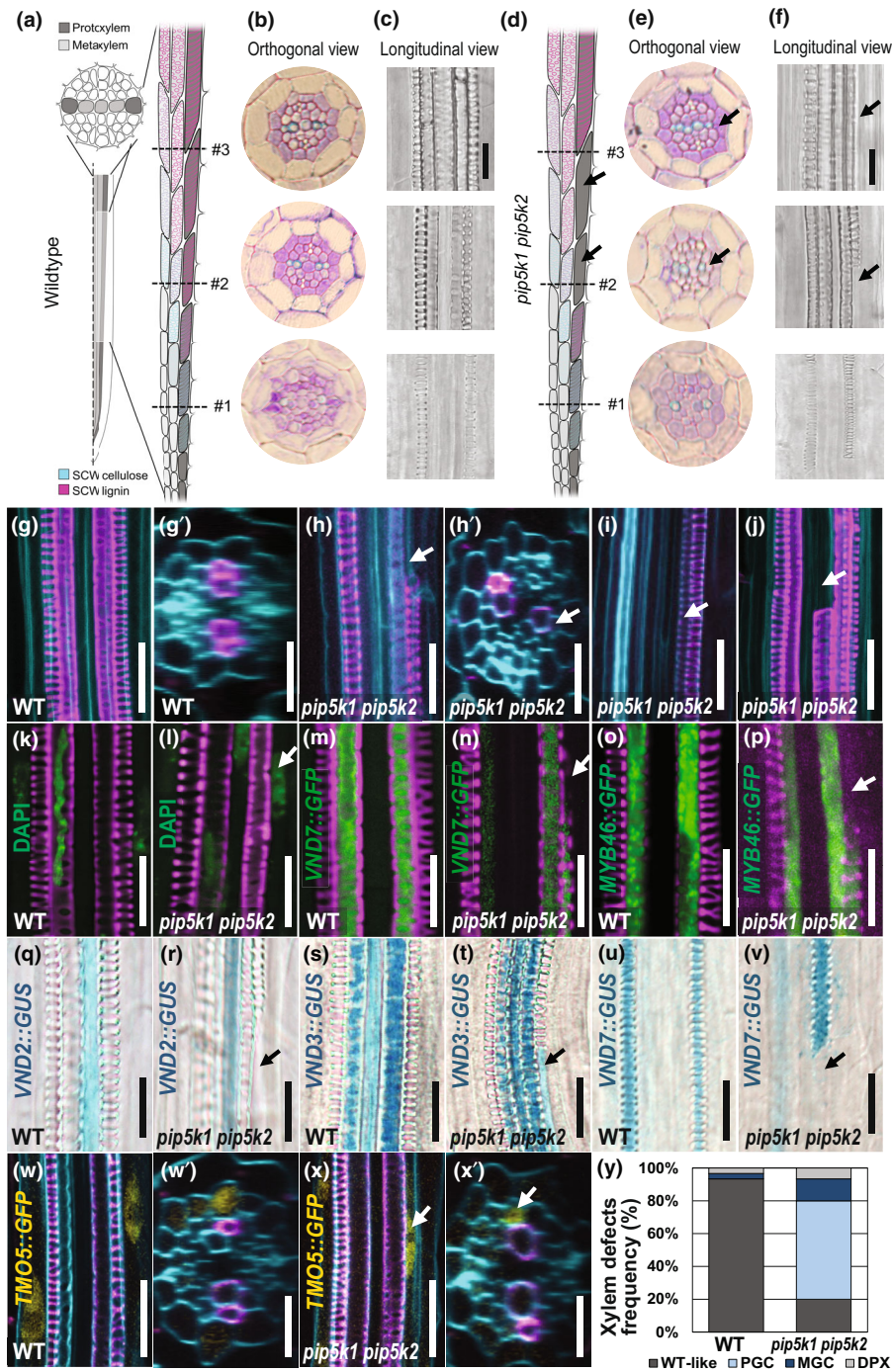


Fig. 1 PIP5K1 and PIP5K2 are essential for correct differentiation of xylem tissues. (a, d) Schematic representations of protoxylem and metaxylem distribution within the primary root of *Arabidopsis thaliana* wild-type (WT) (a) and *pip5k1 pip5k2* (d) plants. The deposition of a secondary cell wall (SCW) of cellulose (cyan) and lignin (magenta) is also displayed in the schemes. (b–f) Orthogonal (b, e) and longitudinal (c, f) views of WT or *pip5k1 pip5k2* roots exhibiting the differentiation of xylem cells. (b, e) Toluidine blue-stained cross-sections exhibiting differentiated protoxylem cells (region #1), first differentiated metaxylem cells (region #2) and a complete differentiation of all xylem strands (region #3) in WT (b) and *pip5k1 pip5k2* (e) roots. (c, f) Bright-field images of 7-d old roots of WT (c) and *pip5k1 pip5k2* (f) plants visualized with a stereoscope microscope. Black arrows mark protoxylem gap cells (PGCs). Bar, 10 μ m. (g–j) Confocal microscopy analysis of protoxylem and metaxylem cells of WT (g, g') and *pip5k1 pip5k2* (h–j) roots stained with Calcofluor White (cyan) and fuchsin (magenta). PGCs (h, h'), double protoxylem (i) and metaxylem gap cells (MGCs, j) can be detected in *pip5k1 pip5k2* roots. White arrows mark gap cells with the exception of (i), where it indicates two protoxylem cells adjacent to each other. (k, l) Nucleus persistence in *pip5k1 pip5k2* roots as evident by the 4',6-diamidino-2-phenylindole dihydrochloride (DAPI)-stained nuclei in fuchsin-stained roots. (m–p) Expression pattern of *VND7::GFP* (m, n) and *MYB46::GFP* (o, p) in *Arabidopsis* roots. Absence of *VND7::GFP* (n) and *MYB46::GFP* (p) expression in *pip5k1 pip5k2* PGCs as revealed by confocal microscopy in fuchsin-stained roots. White arrows mark PGCs. (q–v) Expression analysis of *VND2::GUS* (q, r), *VND3::GUS* (s, t) and *VND7::GUS* (u, v) in WT xylem or *pip5k1 pip5k2* PGCs. Note the presence of *VND3* in PGCs. Black arrows mark PGCs. (w–x') Expression analysis of *TMO5::GFP* in WT and *pip5k1 pip5k2* roots stained with fuchsin (magenta) and Calcofluor White (cyan). (y) Quantification of the frequency of protoxylem and metaxylem defects observed in the roots displayed in (g–j), $n = 50$ seedlings. Bars: (g–x) 20 μ m; (g', h', w', x') 10 μ m.

are present (Figs 1d–f,h,h',y, S1C). To a lesser extent, we also observed breaks in metaxylem strands (metaxylem gap cell, MGC) (Fig. 1j,y) and the emergence of two adjacent protoxylem strands (double protoxylem, DPX) (Fig. 1i,y), indicating that imbalanced PtdIns(4,5)P₂ levels perturb the developmental program of xylem cells. These phenotypes were consistent with PIP5K1 and PIP5K2 distribution within the xylem strands. Fluorescent tagged versions of these proteins (*PIP5K1::PIP5K1:CITRINE* and *PIP5K2::XVE:PIP5K2:YFP*) demonstrated that both enzymes are present in xylem tissues (Fig. S1A–B'). *PIP5K2* expression can be detected at higher intensity in protoxylem cells (Fig. S1B,B'), even if its expression appears slightly broader than *PIP5K1* within the root (Fig. S1A–B'). To further assess the developmental stage of the xylem cells failing to form an SCW in *pip5k1 pip5k2* roots, we analyzed progression of the enucleation process in these cells. Examination of roots stained with fuchsin and DAPI, a fluorescent dye binding DNA regions enriched in adenine–thymine, revealed the presence of intact nuclei in PGCs (Fig. 1k,l), although flanking mature protoxylem elements underwent a normal enucleation process. Next, we examined *VND7* expression in these cells, as this transcription factor controls the signaling cascade regulating xylem differentiation. In WT roots, *VND7* expression as well as the expression of its downstream target *MYB46* precede SCW formation and continue until protoxylem enucleation (Gujas *et al.*, 2017). In contrast to WT roots, analysis of *VND7::GFP*, *VND7::GUS* and *MYB46::GFP* in protoxylem strands of *pip5k1 pip5k2* revealed the absence of both transcription factors in PGCs, suggesting that these cells fail to differentiate (Fig. 1m,p,v). To exclude that PGC phenotypes are not due to a misspecification problem, we examined the expression of *VND7* upstream regulators such as *VND2* and *VND3* transcription factors in xylem cells as well as PGCs (Fig. 1q–t). While *VND2* expression was absent in *pip5k1 pip5k2* PGCs (Fig. 1r), *VND3* expression was clearly detected in PGCs in 17 roots out of 17 PGCs analyzed (Fig. 1t). Additionally, we analyzed the expression of *TARGET OF MONOPTEROS 5 (TMO5)* (De Rybel *et al.*, 2013), which starts to be expressed in the initial developmental stages of xylem formation. Similar to WT roots, *TMO5* expression could be detected

in meristematic xylem strands as well as in PGCs of *pip5k1 pip5k2* (Fig. 1w–x'). These findings indicate that PGCs are competent to acquire protoxylem cell fate but aborted further steps of the xylem differentiation program. Together, our results indicate that PIP5K1 and PIP5K2 participate in the regulation of xylem differentiation.

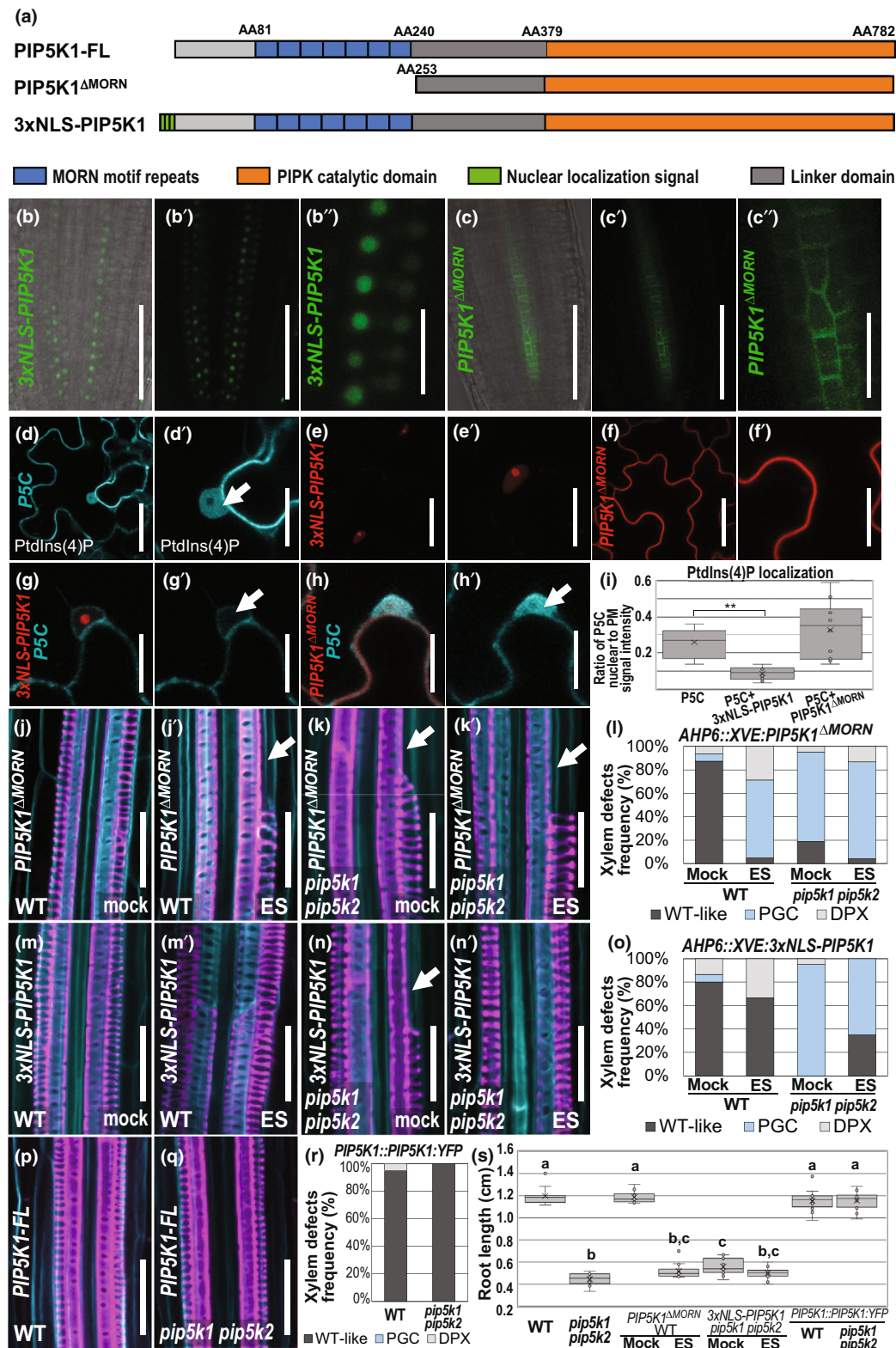
Nuclear PIP5K1 localization is required to promote protoxylem differentiation

Similar to other eukaryotic cells, plant nuclei also contain PtdIns(4,5)P₂ as well as respective biosynthetic enzymes (Mishkind *et al.*, 2009; Dieck *et al.*, 2012), even if the functions of these enzymes in this compartment remain elusive to date. To explore whether the xylem defects observed in *pip5k1 pip5k2* mutants are due to the nuclear activity of these enzymes, we generated reporter-gene fusions for the protoxylem-specific PIP5K1 retaining or excluding it from the nucleus (Fig. 2a). Similar to PIP5K2 (Im *et al.*, 2007; Gerth *et al.*, 2017), where truncation of the N-terminal part including the MORN domain resulted in depletion of the kinase from the nucleus, deletion of the first 252 amino acids located in the seven MORN domains of PIP5K1 (*PIP5K1^{ΔMORN}*) precluded the localization of PIP5K1 into the nucleus (Fig. 2a,b–f'). By contrast, fusion of 3xNLS sequence to the N-termini of PIP5K1 (3xNLS-PIP5K1) led to a nuclear localization of the protein, as evidenced by the CITRINE signal observed in protoxylem cells (Fig. 2b–b"). To test the enzymatic activity of 3xNLS-PIP5K1 and *PIP5K1^{ΔMORN}*, we cotransformed each of them with the PtdIns4P biosensor *UBQ10::2x3xNLS-Pet-1xPH(FAPP1)* (a.k.a. P5C) (Fig. 2d,d'). A decrease in PtdIns4P concentration and therefore enzymatic conversion should translate into a reduction of the fluorescence signal. Indeed, coexpression of P5C with *UBQ::3xNLS-PIP5K1:mCherry* triggered a decrease in P5C specifically in the nucleus (Fig. 2e,e',g,g',i). Instead, coexpression of *UBQ::PIP5K1^{ΔMORN}:mCherry* with the biosensor did not yield significant changes in the P5C nuclear signal, as shown by analysis of the ratio between nuclear and PM signals (Fig. 2f,f',h,h',i). We have previously shown that constitutive expression of *HsPIP5K* is deleterious for correct development of the plant

Fig. 2 Nuclear activity of PIP5K1 regulates the differentiation of protoxylem root cells of *Arabidopsis thaliana*. (a) Schematic representations of the modified versions of PIP5K1 used in this study highlighting the most important protein motifs. (b–c") Subcellular protein localization of 3xNLS-PIP5K1-CITRINE (nuclear-localized, b, b") and *PIP5K1^{ΔMORN}*-CITRINE (excluded from the nucleus, c, c") under the *AHP6::XVE* promoter induced for 6 h. Bars: (b, b', c, c') 100 μm; (b", c") 20 μm. (d–i) Correlation of subcellular distribution of PtdIns(4)P and variants of PIP5K1. Single transient transfection of *Nicotiana benthamiana* epidermal leaves cells with the PtdIns(4)P biosensor P5C (localized in the nucleus and the plasma membrane (PM), d, d'), 3xNLS-PIP5K1-mCherry (e, e') or *PIP5K1^{ΔMORN}*-mCherry (f, f'). Cotransfection of P5C with either 3xNLS-PIP5K1 (g, g') or *PIP5K1^{ΔMORN}* (h, h'). White arrows highlight nuclei. Bars: (d, e, f, g, h) 20 μm; (d', e', f', g', h') 10 μm. (i) Quantification of P5C signal intensity presented as nuclear : PM ratio. Error bars represent ±SD; **, *P* < 0.01 (two tailed paired Student's *t*-test), *n* = 10. Horizontal line indicates median and cross marks the mean value. (j–l) Protoxylem defects observed in wild-type (WT) (j, j') and *pip5k1 pip5k2* (k, k') when inducing *PIP5K1^{ΔMORN}* under inducible, protoxylem-specific AHP6 promoter. Bar, 20 μm. (l) Quantification of the frequency of protoxylem gap cells (PGCs) and double protoxylem observed in the roots represented in (k–j'), *n* = 20 seedlings. (m–o) Protoxylem defects observed in WT (m, m') and *pip5k1 pip5k2* (n, n') when inducing *AHP6::XVE:3xNLS-PIP5K1* (short: 3xNLS-PIP5K1). Bar, 20 μm. White arrows indicate PGCs. (o) Quantification of the frequency of PGCs and double protoxylem observed in the roots represented in (n–o'), *n* = 20 seedlings. (p, q) Full-length PIP5K1 under native/endogenous promoter (short: PIP5K1-FL) leaves xylem development in WT unaffected (p) but complements xylem defects in *pip5k1 pip5k2* fully (q). Bar, 20 μm. (r) Frequency of protoxylem defects observed in WT and *pip5k1 pip5k2* seedlings expressing *PIP5K1::PIP5K1:YFP*, *n* = 20 seedlings. (s) Primary root length of 6-d-old WT and *pip5k1 pip5k2* seedlings expressing different versions of PIP5K1, *n* = 15 roots. Error bars represent ±SD. Statistical significance was evaluated by one-way ANOVA and Tukey's pairwise comparison test. Significant differences (*P* < 0.05) are marked by lowercase letters. Horizontal line indicates median and cross marks the mean value.

(Gujas *et al.*, 2017). To overcome such a limitation, we generated ES-mediated inducible lines harboring both protein versions under control of the protoxylem-specific promoter *ARABIDOPSIS HISTIDINE PHOSPHOTRANSFER 6* (*AHP6*). Interestingly, induction of PIP5K1^{ΔMORN} expression for 6 d in

a WT genetic background mimicked the xylem and root phenotypes observed in *pip5k1 pip5k2* roots whilst slightly aggravating it (Fig. 2j–l,s). An increase in PIP5K1 levels at the PM positively correlated with the emergence of PGCs in 65% of the roots in several transgenic lines analyzed (Fig. 1j–l).



Furthermore, the observed PGCs fail to initiate xylem differentiation processes, as demonstrated by the absence of *VND7* (Fig. S2A–B'). Interestingly, the only-nuclear PIP5K1 version partially restored a continuous protoxylem strand in *c.* 45% of *pip5k1 pip5k2* roots (Fig. 2n,n',o), while protophloem phenotypes and decreased root growth still persisted in the double mutant when ectopically increasing *PIP5K1* in the nucleus (Figs 2s, S2G–M). Remarkably, a greater reduction in PGCs was observed when introducing a full-length version of PIP5K1 (PIP5K1::PIP5K1:YFP) (Watari *et al.*, 2022) in *pip5k1 pip5k2* in comparison to NLS-PIP5K1, suggesting that the nuclear activity of PIP5K1 is required but not solely sufficient to regulate protoxylem differentiation (Fig. 2p–r). Introgression of the FL-PIP5K1 complemented not only root length but also other macroscopic defects reported in *pip5k1 pip5k2* (Fig. 2q–s), consistent with previous findings (Watari *et al.*, 2022). Strikingly, ubiquitous expression of *PIP5K1^{ΔMORN}* in the WT background resulted not only in an increased number of xylem cell files with predominantly spiral SCW pattern (Fig. S2F), but also caused formation of discontinuous protophloem strands and abnormal root hairs (Fig. S2G–I,L,M) while overexpression of 3xNLS-PIP5K1 in the *pip5k1 pip5k2* background was incapable of complementing protophloem discontinuity (Fig. S2I–K). In the WT, vascular tissues seem unaffected by ectopic overexpression of *3xNLS-PIP5K1* (Fig. S2D,I). Together, these findings indicate that the nuclear PIP5K1 activity participates specifically in the regulation of protoxylem differentiation.

Deficient auxin signaling phenocopies the *pip5k1 pip5k2* xylem phenotype

To further explore the underlying molecular mechanisms of the nuclear PIP5K1 activity in protoxylem differentiation, we tested if this effect is related to a perturbed auxin activity. PIP5Ks activities have been proposed to regulate auxin transport through PIN activity (Tejos *et al.*, 2014; Marhava *et al.*, 2020). Hence, we next evaluated if *pip5k1 pip5k2* xylem phenotypes could be related to a decrease in auxin activity in xylem differentiating cells. For this, we took advantage of the previously described *DR5v2-mDII-ntd-Tomato:DR5-DII-n3VENUS* (a.k.a. *R2D2*) auxin reporter, which allows auxin activity to be quantitatively inferred at the single cell level (Liao *et al.*, 2015). Analysis of the mDII : DII ratio in differentiating protoxylem cells before SCW deposition as well as in PGCs revealed a significant decrease of auxin levels in *pip5k1 pip5k2* protoxylem and PGCs in comparison to WT cells (Fig. 3a–c''',u,w). Similar effects on subcellular auxin levels in xylem (gap) cells were observed upon inhibition of auxin polar transport or auxin perception using NPA (Teale & Palme, 2018) and auxinole respectively, whereas NAA treatment resulted in an increased mDII : DII ratio within protoxylem cells (Fig. S3A–D). Furthermore, NPA- and auxinole-induced PGCs express the xylem specification marker *TMO5* (Fig. S3K–M'), indicating that these cells undergo early steps of xylem formation. Interestingly, genetic inhibition of auxin response by means of expressing a dominant negative version of *short hypocotyl 2 (shy2-2)* triggered the formation of PGCs when expressed under the early xylem

promoter *AHP6* (Fig. 3d,e,v). Performing RT-qPCR, we detected a significant decrease in *AHP6* transcript levels upon ES induction of *AHP6::XVE:shy2-2* (Fig. S3T), which could in turn reduce *shy2-2* expression itself. However, the remaining levels of *shy2-2* seem sufficient to induce xylem defects concomitant with those found in NPA- or auxinole-treated plants. By contrast, expression of this gene in more mature xylem cells by the *CELLULOSE BIOSYNTHETIC SUBUNIT A 7 (CESA7)* promoter did not perturb the integrity of protoxylem strands (Fig. 3f,g,v). Despite the absence of *VND7* and *MYB46* (Fig. S3N–O',R,S') expression in the PGCs of plants expressing *AHP6::XVE:shy2-2*, we detected *VND3* expression (Fig. S3P,Q), suggesting that an intact auxin signaling cascade is crucial to induce xylem differentiation but is not required for the specification processes. Together, it appears that *pip5k1 pip5k2* PGCs are the result of disturbed auxin levels in xylem cells before they entered into their differentiation program (Figs 3, S3). To assess whether these defects are due to defective auxin distribution and/or perception, we chemically and genetically impaired both processes and examined their impact on protoxylem formation. To chemically block auxin signaling, we took advantage of auxinole – a molecule that competes with this phytohormone for the binding pocket localized in the SCF^{TIR1} receptor – hindering signal propagation and subsequent auxin response (Strader & Zhao, 2016; Teale & Palme, 2018). Similar to the triple receptor mutant *tir1-1 abf2-1 abf3-1*, confocal microscopy analysis of WT seedlings transferred to plates supplemented with auxinole showed defects in protoxylem tissues, with the presence of PGCs and occasionally double protoxylem strands (Fig. 3j,l,w). Furthermore, neither *VND7* nor *MYB46* expression could be detected in PGCs when blocking auxin perception (Fig. 3o,r), indicating that auxin perception is integral to initiate protoxylem differentiation. Next, we analyzed the phenotypes of plants germinated on plates supplemented with the specific PIN protein blocker NPA. Confocal microscopy analysis of these plants showed a high number of xylem defects (Fig. 3h,m,w), including double protoxylem strands, and a high frequency of PGCs in a similar fashion to *pip5k1 pip5k2*. Consistent with these results, *pin3 pin4 pin7* roots also exhibited PGCs in which the nuclei appeared intact (Fig. 3k). These phenotypes are associated with the lack of *VND7* and *MYB46* expression (Fig. 3p,s), demonstrating that a perturbed auxin transport compromises intracellular auxin flow and, in turn, the auxin-mediated transition from protoxylem maturation to final differentiation.

VND7 expression requires a nuclear PIP5K1-mediated auxin maximum

Recent studies have demonstrated that *VND7* transcript levels must reach a certain threshold to determine the transition of protoxylem cells to terminal differentiation (Turco *et al.*, 2019). While the depletion of *VND7* activity does not interfere with the continuity of protoxylem strands, the simultaneous depletion of *VND7* and *VND6* resulted in the appearance of PGCs (Fig. 4a,c,w; Ramachandran *et al.*, 2021), indicating that *VND7* activates the diverse subcellular events comprising the differentiation

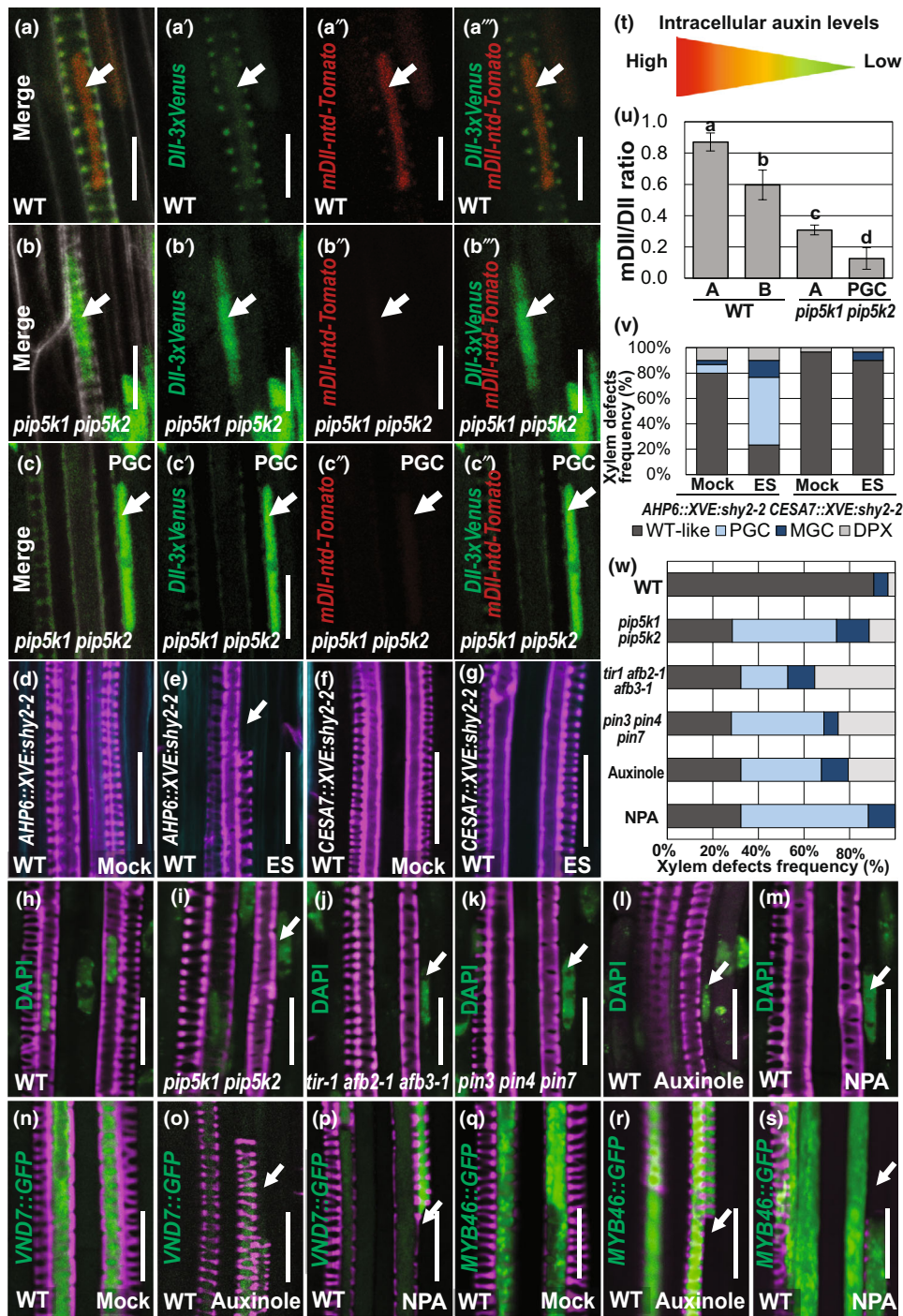


Fig. 3 Intact auxin transport and perception is required to ensure an optimal differentiation of protoxylem cells. (a–c'') Confocal microscopy analysis of protoxylem cells of *Arabidopsis thaliana* wild-type (WT) and *pip5k1 pip5k2* roots stained with Calcofluor White expressing R2D2 dual auxin marker. (a–c) Representative images showing Calcofluor White-stained xylem cells or protoxylem gap cells (PGC) expressing *DR5v2-mDII-ntd-Tomato:DR5-DII-n3VENUS* in WT (a–a'') and *pip5k1 pip5k2* (b–b'') background. a, b and c) display merged images of Calcofluor White staining, *ntdTomato* and *3xNLS-VENUS* (*n3VENUS*) signal while (a', b' and c') show only *n3VENUS* signal, (a'', b'', c'') show *ntd-Tomato* and (a''', b''', c''') display an overlay of *n3VENUS* and *ntd-Tomato*. Bar, 10 μ m. (t) Color-coded representation of the auxin levels in terms of R2D2 fluorescent signal. (u) Graphical depiction of auxin levels in protoxylem cells (a–b'') and PGCs (c–c'') quantified by the ratio between *mDII-ntd-Tomato:DII-n3VENUS*. Error bars represent \pm SD. Statistical significance was evaluated by one-way ANOVA and Tukey's pairwise comparison test. Significant differences ($P < 0.05$) are marked by lowercase letters. (d–g) Representative confocal micrographs of protoxylem cells after inducing *shy2-2* expression for 48 h under *AHP6* (p, q) or *CESA7* (r, s) promoters, respectively. (h–m) Analysis of nuclear persistence in protoxylem cells and PGCs of 4',6-diamidino-2-phenylindole dihydrochloride (DAPI)- and fuchsin-stained roots of the indicated genotypes or wild-type roots treated for 48 h with Auxinole or 1-N-naphthylphthalamic acid (NPA). (n–s) Analysis of *VND7* or *MYB46* expression in protoxylem cells of WT roots transferred for 48 h to media containing auxinole or NPA. (v–w) Quantification of xylem defects observed in the indicated genotypes calculated as the frequency of the phenotypes observed per root; $n = 30$. White arrows mark PGCs. Bar, 20 μ m unless stated otherwise.

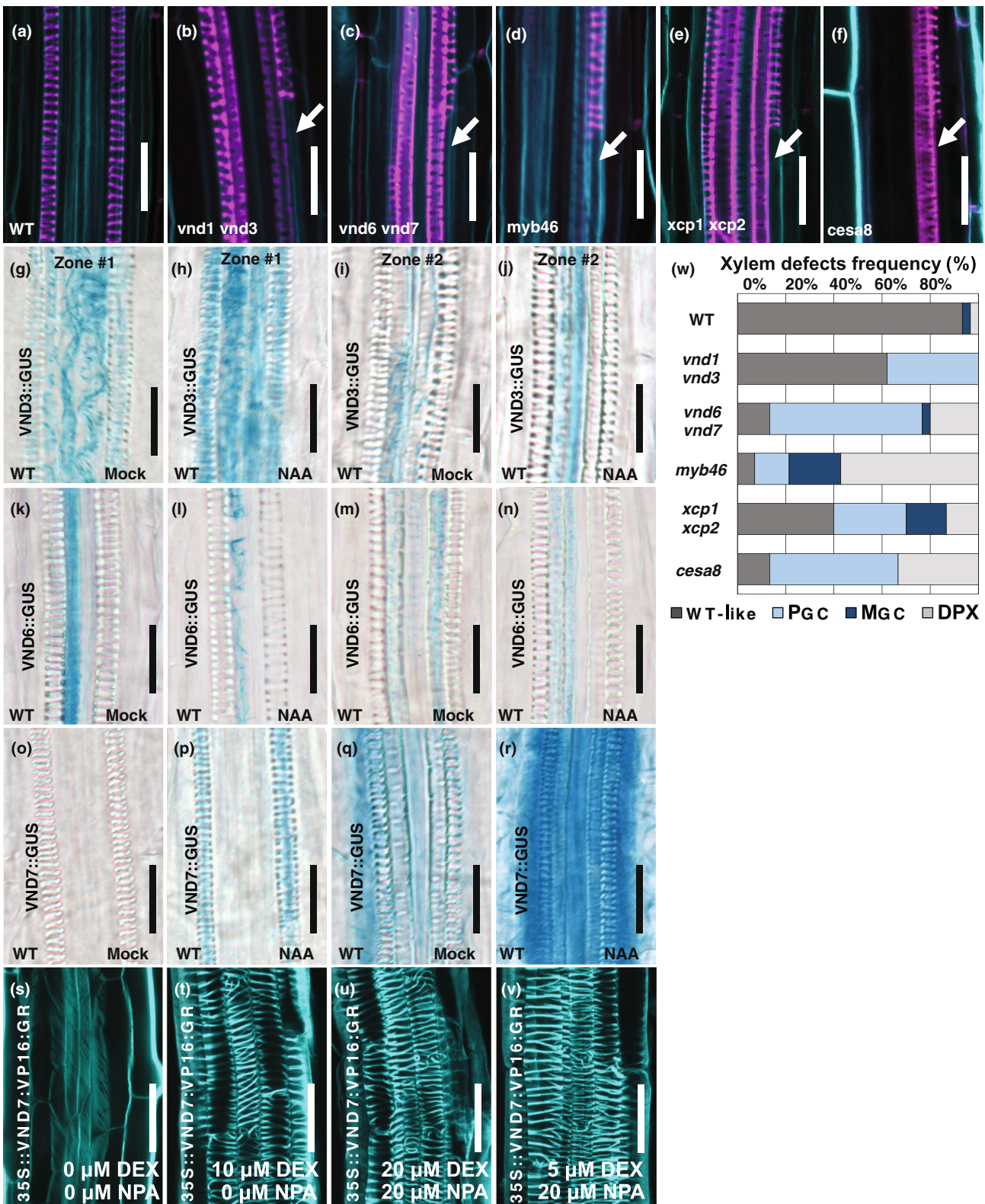


Fig. 4 VND7 induction by auxin modulates the differentiation of xylem cells of *Arabidopsis thaliana*. (a–f) Confocal microscopy analysis of protoxylem and metaxylem strands in Calcofluor White- and fuchsin-stained roots of the indicated genotypes. White arrows mark protoxylem gap cells (PGCs). Bar, 20 μ m. (w) Quantification of xylem defects observed in the roots represented in (a–f). $n = 35$. (g–r) GUS staining of xylem cells expressing VND3::GUS (g–j), VND6::GUS (k–n) and VND7::GUS (o–r) in wild-type roots under mock conditions or transferred for 3 h to medium containing 10 μ M NAA. Bar, 20 μ m. (s–v) Xylem transdifferentiation assays performed in 35S::VND7:VN16:GR roots transferred to media supplemented with 0, 5, 10 or 20 μ M dexamethasone (DEX) and 20 μ M NPA for 24 h. Bar, 20 μ m.

program of protoxylem cells. Consistent with this, interference with activity of the well-described *VND7* downstream targets *XYLEM CYSTEINE PEPTIDASE (XCP) 1*, *XCP2*, *MYB46*, *CELLULOSE SYNTHASE (CESA) 8* disturbed protoxylem differentiation, as evident by the occasional appearance of PGCs (Fig. 4d–f,w). To a lesser extent, the appearance of PGCs was found in the double mutant of the *VND7*-homologs *vnd1 vnd3* (Fig. 4b,w), but the predominant xylem phenotype we observed in these seedlings was an evident delay in metaxylem formation as described recently by Ramachandran *et al.* (2021) (Fig. 4w). Given that the xylem phenotypes observed in these mutants are reminiscent of those observed in *pip5k1 pip5k2* roots, we next determined if an induction of *VND7* expression responds to an increase in auxin concentration. To this end, we first tested how *VND7* expression reacts to exogenous auxin application. *VND7::GUS* 6-d-old seedlings were treated with 10 μ M NAA (a synthetic homolog of auxin) for 3 h. An increase in *VND7* expression was observed in regions 1 and 2 of the roots (Figs 1a, 4o–r).

In comparison, *VND3* as well as *VND6* expression remained unaltered in NAA-treated seedlings (Fig. 4g–n). To further demonstrate that auxin signaling cues converge with the *VND7* signaling cascade, we sought to induce protoxylem differentiation when blocking auxin activity. For this, we used the previously described DEX inducible system that promotes xylem transdifferentiation in all root cells upon DEX-mediated *VND7* induction (Watanabe *et al.*, 2018). As expected, 48 h of incubation in $\frac{1}{2}$ MS media containing 0, 5, 10 and 20 μ M DEX triggered the transdifferentiation of epidermal cells, as manifested by the SCW observed in these cells (Fig. 4s,t). Blockage of auxin transport by adding 20 μ M NPA to the medium concomitant with *VND7* induction did not prevent the transdifferentiation of the epidermal cells (Fig. 4u,v), demonstrating that *VND7* activation is sufficient to trigger xylem differentiation despite blockage of auxin flow. To further evaluate whether auxin accumulation is a prerequisite for *VND7*-mediated differentiation of xylem cells, we boosted the auxin concentration in *pip5k1 pip5k2* protoxylem

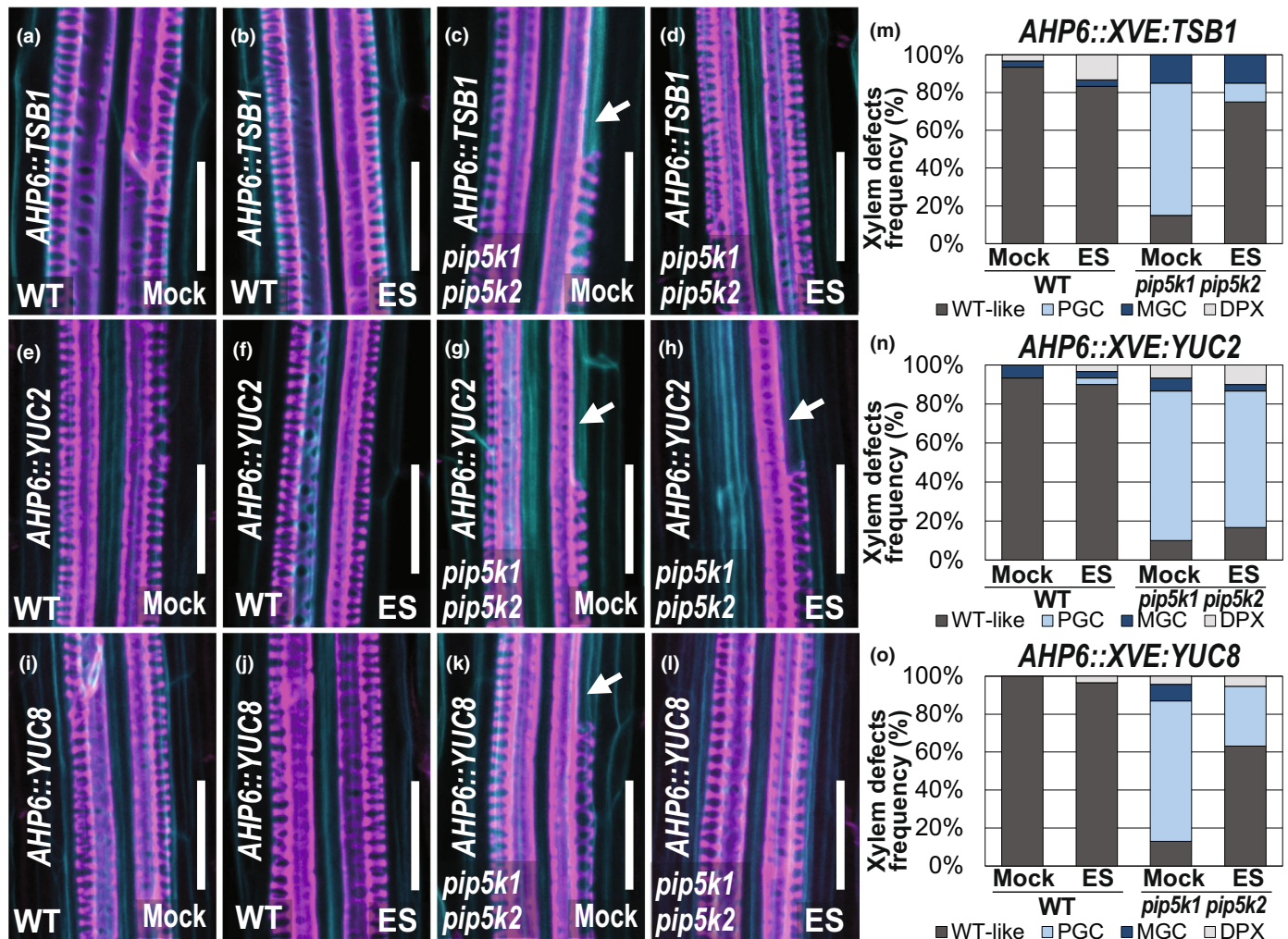


Fig. 5 Xylem-specific expression of auxin biosynthetic genes partially rescues *pip5k1 pip5k2* protoxylem defects in *Arabidopsis thaliana*. (a–l) Xylem-specific induction of *TSB1* (a–d), *YUCCA 2 (YUC2)* (e–h) and *YUCCA8 (YUC8)* (i–l) in wild-type and *pip5k1 pip5k2* roots. Four-day-old seedlings were transferred for 48 h to a medium containing 2 μ M ES and immediately fixed and stained with fuchsin and Calcofluor White before confocal microscopy visualization. White arrows mark protoxylem gap cells (PGCs). Bar, 20 μ m. (m–o) Quantification of xylem defects in 6-d-old seedlings germinated on 2 μ M ES expressing *TSB1* (m), *YUCCA2* (n) and *YUCCA8* (o) under the inducible *AHP6* promoter. $n = 35$.

strands. The protoxylem-specific induction of the early auxin biosynthetic enzyme TRYPTOPHAN BETA SUBUNIT 1 (TSB1, Fig. 5a,b,m; Ursache *et al.*, 2014), YUCCA2 (Fig. 5e,f,n) and YUCCA8 (Fig. 5i,j,o) in a WT background had no impact on xylem development (Fig. 5). Remarkably, induction of TSB1 (Fig. 5c,d,m) and YUCCA8 (Fig. 5k,l,o) but not *YUCCA2* (Fig. 5g,h,n) in protoxylem cells of *pip5k1 pip5k2* partially suppressed PGC emergence, reinforcing the notion that an auxin maximum needs to be established to induce *VND7* expression and, in turn, initiate protoxylem differentiation. Together, our results demonstrated that the bipartite PIP5K1 activities at the PM and the nucleus are necessary to boost auxin levels, which in turn control the onset of protoxylem differentiation programs.

Discussion

Nuclear and PM-residence of PIP5K1 are integral for xylem differentiation

In recent years, studies of the regulation of developmental programs exerted by phosphoinositides have begun to emerge (Gujas *et al.*, 2017; Platre *et al.*, 2019). The enrichment of certain phosphoinositide species at the PM has been associated with correct progression of the developmental trajectory of root hairs or vascular cells (Gujas *et al.*, 2017; Platre *et al.*, 2019). Despite membrane-associated phosphoinositides, a distinct nucleolar pool including envelope-bound as well as nucleoplasmic phosphoinositides has been described (Champeyroux *et al.*, 2020). Although there is wide knowledge about the role of nuclear phosphoinositides in other species/organisms remodeling chromatin structure (Hamann & Blind, 2018; Fiume *et al.*, 2019) and their importance for human health (Choi *et al.*, 2019), plant research has largely neglected nuclear phosphoinositides with only a handful of articles covering the subject (Dieck *et al.*, 2012; Gerth *et al.*, 2017; Champeyroux *et al.*, 2020). Our findings here highlight for the first time the additive regulation of protoxylem differentiation by the nuclear and PM activity of PIP5K1. Similar to its homolog PIP5K2, PIP5K1 exhibits seven MORN domains responsible for its nuclear localization that are integral to the regulation of xylem differentiation programs (Fig. 2; Gerth *et al.*, 2017). *pip5k1 pip5k2* double mutants displayed defects in xylem continuity, as evidenced by the appearance of PGCs (Fig. 1). Detailed examination of PGCs showed that their nuclei remain intact, which together with the absence of *VND7* and *MYB46* expression indicate that these cells failed to differentiate (Fig. 1). Introgression of an only-nuclear version of PIP5K1 reduced the emergence of PGCs in *pip5k1 pip5k2* roots by 45%. Instead, WT plants with an increased dosage of PIP5K1 at the PM showed discontinuities in their protoxylem strands. While low native expression levels of PIP5K1 in protoxylem cells prevent the determination of its exact subcellular localization in these tissues (Fig. S1), analysis in transiently transfected tobacco cells has shown its PM localization, consistent with previous reports in *Arabidopsis* epidermal cells (Ischebeck *et al.*, 2013; Tejos *et al.*, 2014). These results suggest not only that a tight balance of PtdIns(4,5)P₂ is required to modulate xylem differentiation but

also that an optimal subcompartmentalization of their biosynthetic enzymes is crucial to properly regulate this process. Yet, the function of nuclear phosphoinositides is poorly characterized. Introgression of the human PIP5K1 counterpart (*HsPIP5K1α*) in tobacco cells decreased the DNA replication rate as well as histone acetylation (Dieck *et al.*, 2012). The latter reflects a noncondensed chromatin stage, which is necessary to promote gene transcription. Unlike in plants, mutations in *PIP5K* orthologs in animal cells translated into transcriptional defects (Chakrabarti *et al.*, 2015). Hence, it appears possible that the nuclear residence of PIP5K1 contributes to modulate chromatin architecture and, in turn, the transcriptional rate of xylem master regulators such as *VND7*. However, further experiments are necessary to confirm this hypothesis.

Auxin activation of VND7 controls the onset of protoxylem differentiation

Our findings additionally demonstrated that an increase in auxin levels occurs before the initiation of protoxylem differentiation. It is well accepted that the distribution of auxin and cytokinin delineates the vascular pattern of the root vascular tissues (Vaughan-Hirsch *et al.*, 2018). Indeed, a genetic or chemical alteration of auxin activity results in the appearance of an additional protoxylem strand at the procambium position (Fig. 3), a phenotype that we also observed when interfering with PIP5K1 and PIP5K2 function (Figs 1i,y, S2F). While auxin triggers the specification of protoxylem and metaxylem cells (De Rybel *et al.*, 2014; Ursache *et al.*, 2014), its role in modulating the differentiation of both tissues is poorly described. Suppression of auxin perception by expressing *shy2-2* in early protoxylem cells abolished the onset of the differentiation program of these cells, a phenotype never observed when expressing this gene in differentiating protoxylem cells (Fig. 3g,v). Thus, it appears that an intact auxin response within meristematic xylem cells is necessary to ensure their optimal differentiation. This idea is reinforced by the presence of PGCs in the xylem strands of *tir1 afb2 afb3* and auxinole-treated roots (Fig. 3j,l). Consistent with previous studies, our observations demonstrated that a chemical or genetic blockage within the root is modulated by the polarly localized PIN transporters, which canalized auxin unidirectionally and promoted the formation of an auxin maximum at specific locations (Scarpella *et al.*, 2006; Mazur *et al.*, 2020a). Increasing the expression of a nuclear-excluded version of PIP5K1 in WT plants triggers the formation of several xylem defects. Notably, *PIP5K1* and *PIP5K2* expression are enhanced by external auxin application in root epidermal cells, creating a potential scenario in which an optimal concentration of PtdIns(4,5)P₂ allows a sustained auxin flow through xylem tissues (Ischebeck *et al.*, 2013; Tejos *et al.*, 2014). In fact, evaluation of auxin levels in the first cells entering xylem differentiation upon inhibition of auxin transport revealed a reduced amount of the phytohormone present in these cells (Fig. S3D). Previous studies have demonstrated that tryptophan-dependent auxin biosynthesis is crucial for the specification of metaxylem cells (Ursache *et al.*, 2014). Together, our findings imply that the establishment

of an auxin maximum in dividing meristematic protoxylem cells is necessary not only to safeguard the correct xylem patterning but also to modulate the entry of protoxylem cells into their differentiation programs. The suppression of PGCs in *pip5k1 pip5k2* roots by the xylem-specific induction of auxin biosynthetic enzymes such as *TSB1* or *YUCCA8* corroborates this hypothesis (Fig. 5m,o).

Maintenance of an auxin peak during xylem differentiation would hence promote the expression of xylem differentiation regulators such as *VND7*. In agreement with this hypothesis, *VND7* expression was abolished in PGCs, which resulted from treatment with the auxin transport inhibitor NPA (Fig. 4). We also showed that auxin boosts *VND7* transcription in the root meristematic region (Fig. 4p), which in turn is necessary to activate the downstream signaling cascade regulating SCW deposition and vacuole-driven programmed cell death (Escamez & Tuominen, 2014). Indeed, a deficient activity of XCP enzymes or CESA8 proteins led to protoxylem breaks reminiscent of *pip5k1 pip5k2* (Fig. 4w), reinforcing the idea that the latter defects are due to an insufficient auxin-mediated activation of *VND7*. While at this stage our studies cannot confirm this hypothesis, the presence of *VND3* in *pip5k1 pip5k2* PGCs (Fig. 1t) suggests that distinct cues regulate VND factors to ensure *VND7* activation. Consistent with a recent publication, our results demonstrated that intact activities of the *VND7*-upstream factors *VND1* and *VND3* are necessary to modulate the correct differentiation of metaxylem cells (Fig. 4b; Ramachandran *et al.*, 2021). Transcriptional analysis of ABA-deficient mutants demonstrated that this hormone contributes to modulate *VND3* expression among other genes involved in the regulation of xylem cells. Indeed, the activity of this gene is essential to ensure proto- and metaxylem patterning in ABA-treated plants. In contrast to *VND7*, *VND3* expression was not enhanced upon NAA treatment (Fig. 4h,j). Together with *VND3* expression in *pip5k1 pip5k2* cells, it seems that auxin-mediated regulation of protoxylem differentiation via *VND7* activation depends on other auxin-related factors beyond the VND family. While *VND7* activation is sufficient to trigger the irreversible differentiation of xylem cells, the induction of distinct VND factors by different developmental and environmental cues such as ABA and auxin contributes to safeguard the plasticity of xylem cells.

Acknowledgements

CM and TMDC were funded by PSC-Syngenta Research Fellowship Program and ETH-Foundation fellowships respectively. This work was funded by the Swiss National Foundation (SNF_31003A_160201) to AR-V. We thank Thomas Greb, Jiri Friml, Taku Demura, Annelie Carlsbecker, Takashi Aoyama, Bert de Rybel and Clara Sanchez-Rodriguez for kindly providing seeds. We also thank Elisabeth Truernit for critical reading of the manuscript. The authors gratefully acknowledge ScopeM for their support and assistance in this work and thank Kai Kirchoff for excellent technical support. Open access funding provided by Eidgenössische Technische Hochschule Zurich. Open access funding provided by Eidgenössische Technische Hochschule Zurich.


Competing interests


None declared.


Author contributions

CM, TMDC and AR-V designed the research and wrote the manuscript. CM, TMDC and NB-T performed the experiments.

ORCID

Noel Blanco-Touriñan  <https://orcid.org/0000-0003-4610-6110>

Claudia Mark von der  <https://orcid.org/0000-0003-4338-5265>

Antia Rodriguez-Villalon  <https://orcid.org/0000-0001-8962-1353>

Data availability

All data and material that support the findings of this study are available upon request from the corresponding authors.

References

- Bishopp A, Help H, El-Showk S, Weijers D, Scheres B, Friml J, Benkova E, Mahonen AP, Helariutta Y. 2011. A mutually inhibitory interaction between auxin and cytokinin specifies vascular pattern in roots. *Current Biology* 21: 917–926.
- Bollhoner B, Prestele J, Tuominen H. 2012. Xylem cell death: emerging understanding of regulation and function. *Journal of Experimental Botany* 63: 1081–1094.
- Cano-Delgado A, Lee JY, Demura T. 2010. Regulatory mechanisms for specification and patterning of plant vascular tissues. *Annual Review of Cell and Developmental Biology* 26: 605–637.
- Chakrabarti R, Sanyal S, Ghosh A, Bhar K, Das C, Siddhanta A. 2015. Phosphatidylinositol-4-phosphate 5-kinase 1 α modulates ribosomal RNA gene silencing through its interaction with histone H3 lysine 9 trimethylation and heterochromatin protein HP1- α . *The Journal of Biological Chemistry* 290: 20893–20903.
- Champeyroux C, Stoof C, Rodriguez-Villalon A. 2020. Signaling phospholipids in plant development: small couriers determining cell fate. *Current Opinion in Plant Biology* 57: 61–71.
- Choi S, Chen M, Cryns VL, Anderson RA. 2019. A nuclear phosphoinositide kinase complex regulates p53. *Nature Cell Biology* 21: 462–475.
- Czechowski T, Stitt M, Altmann T, Udvardi MK, Scheible WR. 2005. Genome-wide identification and testing of superior reference genes for transcript normalization in Arabidopsis. *Plant Physiology* 139: 5–17.
- De Rybel B, Adibi M, Breda AS, Wendrich JR, Smit ME, Novak O, Yamaguchi N, Yoshida S, Van Isterdael G, Palovaara J *et al.* 2014. Plant development. Integration of growth and patterning during vascular tissue formation in Arabidopsis. *Science* 345: 1255215.
- De Rybel B, Mahonen AP, Helariutta Y, Weijers D. 2016. Plant vascular development: from early specification to differentiation. *Nature Reviews Molecular Cell Biology* 17: 30–40.
- De Rybel B, Möller B, Yoshida S, Grabowicz I, Barbier de Reuille P, Boeren S, Smith RS, Borst JW, Weijers D. 2013. A bHLH complex controls embryonic vascular tissue establishment and indeterminate growth in Arabidopsis. *Developmental Cell* 24: 426–437.
- Dieck CB, Wood A, Brglez I, Rojas-Pierce M, Boss WF. 2012. Increasing phosphatidylinositol (4,5) biphosphate biosynthesis affects plant nuclear lipids and nuclear functions. *Plant Physiology and Biochemistry* 57: 32–44.

- Dolan L, Janmaat K, Willemsen V, Linstead P, Poethig S, Roberts K, Scheres B. 1993. Cellular organisation of the *Arabidopsis thaliana* root. *Development* 119: 71–84.
- Endo H, Yamaguchi M, Tamura T, Nakano Y, Nishikubo N, Yoneda A, Kato K, Kubo M, Kajita S, Katayama Y *et al.* 2015. Multiple classes of transcription factors regulate the expression of VASCULAR-RELATED NAC-DOMAIN7, a master switch of xylem vessel differentiation. *Plant & Cell Physiology* 56: 242–254.
- Escamez S, Tuominen H. 2014. Programmes of cell death and autolysis in tracheary elements: when a suicidal cell arranges its own corpse removal. *Journal of Experimental Botany* 65: 1313–1321.
- Fiume R, Faenza I, Sheth B, Poli A, Vidalle MC, Mazzetti C, Abdul SH, Campagnoli F, Fabbrini M, Kimber ST *et al.* 2019. Nuclear phosphoinositides: their regulation and roles in nuclear functions. *International Journal of Molecular Sciences* 20: 2991.
- Friml J, Vieten A, Sauer M, Weijers D, Schwarz H, Hamann T, Offringa R, Jurgens G. 2003. Efflux-dependent auxin gradients establish the apical-basal axis of *Arabidopsis*. *Nature* 426: 147–153.
- Gerth K, Lin F, Daamen F, Menzel W, Heinrich F, Heilmann M. 2017. *Arabidopsis* phosphatidylinositol 4-phosphate 5-kinase 2 contains a functional nuclear localization sequence and interacts with alpha-importins. *The Plant Journal* 92: 862–878.
- Gujas B, Cruz TMD, Kastanaki E, Vermeer JEM, Munnik T, Rodriguez-Villalon A. 2017. Perturbing phosphoinositide homeostasis oppositely affects vascular differentiation in *Arabidopsis thaliana* roots. *Development* 144: 3578–3589.
- Hamann BL, Blind RD. 2018. Nuclear phosphoinositide regulation of chromatin. *Journal of Cellular Physiology* 233: 107–123.
- Haseloff J. 1999. GFP variants for multispectral imaging of living cells. *Methods in Cell Biology* 58: 139–151.
- Im YJ, Davis AJ, Perera IY, Johannes E, Allen NS, Boss WF. 2007. The N-terminal membrane occupation and recognition nexus domain of *Arabidopsis* phosphatidylinositol phosphate kinase 1 regulates enzyme activity. *The Journal of Biological Chemistry* 282: 5443–5452.
- Ischebeck T, Werner S, Krishnamoorthy P, Lerche J, Meijon M, Stenzel I, Lofke C, Wiessner T, Im YJ, Perera IY *et al.* 2013. Phosphatidylinositol 4,5-bisphosphate influences PIN polarization by controlling clathrin-mediated membrane trafficking in *Arabidopsis*. *Plant Cell* 25: 4894–4911.
- Jang G, Chang SH, Um TY, Lee S, Kim JK, Choi YD. 2017. Antagonistic interaction between jasmonic acid and cytokinin in xylem development. *Scientific Reports* 7: 10212.
- Jefferson RA, Kavanagh TA, Bevan MW. 1987. GUS fusions: beta-glucuronidase as a sensitive and versatile gene fusion marker in higher plants. *EMBO Journal* 6: 3901–3907.
- Kastanaki E, Blanco-Touriñán N, Sarazin A, Sturchler A, Gujas B, Vera-Sirera F, Agusti J, Rodriguez-Villalon A. 2022. A genetic framework for proximal secondary vein branching in the *Arabidopsis thaliana* embryo. *Development* 149: dev200403.
- Kim WC, Ko JH, Kim JY, Kim J, Bae HJ, Han KH. 2013. MYB46 directly regulates the gene expression of secondary wall-associated cellulose synthases in *Arabidopsis*. *The Plant Journal* 73: 26–36.
- Kubo M, Udagawa M, Nishikubo N, Horiguchi G, Yamaguchi M, Ito J, Mimura T, Fukuda H, Demura T. 2005. Transcription switches for protoxylem and metaxylem vessel formation. *Genes & Development* 19: 1855–1860.
- Kurihara D, Mizuta Y, Sato Y, Higashiyama T. 2015. ClearSee: a rapid optical clearing reagent for whole-plant fluorescence imaging. *Development* 142: 4168–4179.
- Liao CY, Smet W, Brunoud G, Yoshida S, Vernoux T, Weijers D. 2015. Reporters for sensitive and quantitative measurement of auxin response. *Nature Methods* 12: 207–210.
- Lucas WJ, Groover A, Lichtenberger R, Furuta K, Yadav SR, Helariutta Y, He XQ, Fukuda H, Kang J, Brady SM *et al.* 2013. The plant vascular system: evolution, development and functions. *Journal of Integrative Plant Biology* 55: 294–388.
- Marhava P, Aliaga Fandino AC, Koh SWH, Jelinkova A, Kolb M, Janacek DP, Breda AS, Cattaneo P, Hammes UZ, Petrsek J *et al.* 2020. Plasma membrane domain patterning and self-reinforcing polarity in *Arabidopsis*. *Developmental Cell* 52: 223–235.
- Mazur E, Gallei M, Adamowski M, Han HB, Robert HS, Friml J. 2020a. Clathrin-mediated trafficking and PIN trafficking are required for auxin canalization and vascular tissue formation in *Arabidopsis*. *Plant Science* 293: 110414.
- Mazur E, Kulik I, Hajny J, Friml J. 2020b. Auxin canalization and vascular tissue formation by TIR1/AFB-mediated auxin signaling in *Arabidopsis*. *New Phytologist* 226: 1375–1383.
- Mishkind M, Vermeer JE, Darwish E, Munnik T. 2009. Heat stress activates phospholipase D and triggers PIP accumulation at the plasma membrane and nucleus. *The Plant Journal* 60: 10–21.
- Norkunas K, Harding R, Dale J, Dugdale B. 2018. Improving agroinfiltration-based transient gene expression in *Nicotiana benthamiana*. *Plant Methods* 14: 71.
- Oda Y, Fukuda H. 2012. Secondary cell wall patterning during xylem differentiation. *Current Opinion in Plant Biology* 15: 38–44.
- Platre MP, Bayle V, Armengot L, Bareille J, Marques-Bueno MDM, Creff A, Maneta-Peyret L, Fiche JB, Nollmann M, Mieg C *et al.* 2019. Developmental control of plant Rho GTPase nano-organization by the lipid phosphatidylserine. *Science* 364: 57–62.
- Ramachandran P, Augstein F, Mazumdar S, Nguyen TV, Minina EA, Melnyk CW, Carlsbecker A. 2021. Abscisic acid signaling activates distinct VND transcription factors to promote xylem differentiation in *Arabidopsis*. *Current Biology* 31: 3153–3161.
- Rodriguez-Villalon A, Gujas B, van Wijk R, Munnik T, Hardtke CS. 2015. Primary root protophloem differentiation requires balanced phosphatidylinositol-4,5-bisphosphate levels and systemically affects root branching. *Development* 142: 1437–1446.
- Ruonala R, Ko D, Helariutta Y. 2017. Genetic networks in plant vascular development. *Annual Review of Genetics* 51: 335–359.
- Scarpella E, Marcos D, Friml J, Berleth T. 2006. Control of leaf vascular patterning by polar auxin transport. *Genes & Development* 20: 1015–1027.
- Strader LC, Zhao Y. 2016. Auxin perception and downstream events. *Current Opinion in Plant Biology* 33: 8–14.
- Teale W, Palme K. 2018. Naphthylphthalamic acid and the mechanism of polar auxin transport. *Journal of Experimental Botany* 69: 303–312.
- Tejos R, Sauer M, Vanneste S, Palacios-Gomez M, Li H, Heilmann M, van Wijk R, Vermeer JE, Heilmann I, Munnik T *et al.* 2014. Bipolar plasma membrane distribution of phosphoinositides and their requirement for auxin-mediated cell polarity and patterning in *Arabidopsis*. *Plant Cell* 26: 2114–2128.
- Turco GM, Rodriguez-Medina J, Siebert S, Han D, Valderrama-Gomez MA, Vahldick H, Shulse CN, Cole BJ, Juliano CE, Dickel DE *et al.* 2019. Molecular mechanisms driving switch behavior in xylem cell differentiation. *Cell Reports* 28: 342–351.
- Ursache R, Miyashima S, Chen Q, Vaten A, Nakajima K, Carlsbecker A, Zhao Y, Helariutta Y, Dettmer J. 2014. Tryptophan-dependent auxin biosynthesis is required for HD-ZIP III-mediated xylem patterning. *Development* 141: 1250–1259.
- Vaughan-Hirsch J, Goodall B, Bishopp A. 2018. North, East, South, West: mapping vascular tissues onto the *Arabidopsis* root. *Current Opinion in Plant Biology* 41: 16–22.
- Vermeer JE, von Wangenheim D, Barberon M, Lee Y, Stelzer EH, Maizel A, Geldner N. 2014. A spatial accommodation by neighboring cells is required for organ initiation in *Arabidopsis*. *Science* 343: 178–183.
- Watanabe Y, Schneider R, Barkwill S, Gonzales-Vigil E, Hill JL Jr, Samuels AL, Persson S, Mansfield SD. 2018. Cellulose synthase complexes display distinct dynamic behaviors during xylem transdifferentiation. *Proceedings of the National Academy of Sciences, USA* 115: E6366–E6374.
- Watari M, Kato M, Blanc-Mathieu R, Tsuge T, Ogata H, Aoyama T. 2022. Functional differentiation among the *Arabidopsis* phosphatidylinositol 4-phosphate 5-kinase genes PIP5K1, PIP5K2 and PIP5K3. *Plant & Cell Physiology* 63: 635–648.
- Yamaguchi M, Kubo M, Fukuda H, Demura T. 2008. Vascular-related NAC-DOMAIN7 is involved in the differentiation of all types of xylem vessels in *Arabidopsis* roots and shoots. *The Plant Journal* 55: 652–664.

Zhong R, Lee C, Ye ZH. 2010. Global analysis of direct targets of secondary wall NAC master switches in *Arabidopsis*. *Molecular Plant* 3: 1087–1103.

Supporting Information

Additional Supporting Information may be found online in the Supporting Information section at the end of the article.

Fig. S1 *PIP5K1* and *PIP5K2* distribution in xylem tissues of *Arabidopsis* roots and subcellular localization in *Nicotiana benthamiana*.

Fig. S2 Vascular phenotypes upon induction of *PIP5K1*^{AMORN} and *NLS-PIP5K1* expression.

Fig. S3 Perturbed auxin transport and response impairs protoxylem differentiation in *Arabidopsis thaliana* roots.

Table S1 List of primers used in this study.

Please note: Wiley Blackwell are not responsible for the content or functionality of any Supporting Information supplied by the authors. Any queries (other than missing material) should be directed to the *New Phytologist* Central Office.